JACS
JOURNAL OF THE AMERICAN CHEMICAL SOCIETY

Article

pubs.acs.org/JACS

Fluorinated Boron Nitride Nanotube Quantum Dots: A Spin Filter

Kamal B. Dhungana and Ranjit Pati*

Department of Physics, Michigan Technological University, Houghton, Michigan 49931, United States

Supporting Information

ABSTRACT: Spin filtering requires a selective transmission of spin-polarized carriers. A perfect spin filter allows all majority (or minority) spin carriers to pass through a *channel* while blocking the minority (or majority) carriers. The quest for a novel low-dimensional metal-free magnetic material that would exhibit magnetism at a higher temperature with an excellent spin filtering property has been intensively pursued. Herein, using a first-principles approach, we demonstrate that the fluorinated boron nitride nanotube (F-BNNT) quantum dot, which is ferromagnetic in nature, can be used as a perfect spin filter with efficiency as high as 99.8%. Our calculation shows that the ferromagnetic spin ordering in F-BNNT is stable at a higher temperature. Comparison of the conductance value of the F-BNNT quantum dot with that of the pristine BNNT quantum dot reveals a significantly higher conductance in F-BNNT, which is in very good agreement with the experimental report (Tang, C., et al. *J. Am. Chem. Soc.* **2005**, *127*, 6552).

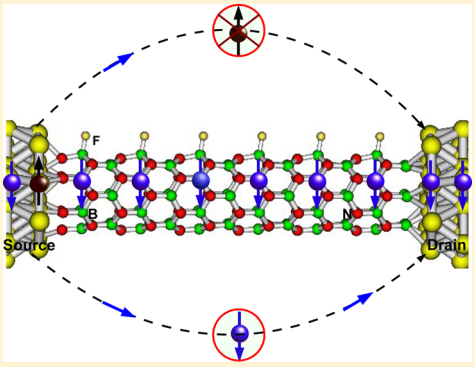

INTRODUCTION

Since their inception, carbon nanotubes (CNTs)[1] and boron nitride nanotubes (BNNTs)[2−4] have received enormous attention due to their novel properties and possible applications in nanoelectronics. Despite structural similarities, there are vast differences between them in terms of electronic and physical properties.[5,6] CNTs exhibit chiral-dependent electronic properties; based upon the chirality, they can be metallic or semiconducting. On the other hand, electronic properties of BNNTs do not rely on chirality, but their high electrical resistivity due to their large band gap makes them unsuitable for several electronic device applications. The most convenient way to circumvent this issue associated with the BNNTs is to modify their electronic structure by functionalizing, doping, and filling them with suitable candidates.[7] In the past few years, with this route, a large number of experimental and theoretical investigations have been carried out to synthesize, predict, and modify the electronic structure of the BNNTs.[8−14] Out of the several proposed methods, doping and surface chemisorption are found to be more appealing techniques for tuning the electronic properties of the BNNTs.[15]

For example, in a pioneering attempt, Tang et al. reported the synthesis of fluorinated BNNTs using a novel technique, where they introduced fluorine atoms during the tube growth.[15] They found the resistivity of the F-BNNT to be about 3 orders of magnitude smaller than that of the pristine BNNT; fluorinated BNNT has also been shown to exhibit p-type semiconducting behavior.[16] Soon after the experimental realization, based on a first-principles approach, Li and co-workers first showed that the chemisorption of fluorine can induce spontaneous magnetization.[17] In another instance, Zhang et al. have shown for the first time that fluorine atoms adsorbed on BNNT can induce long-ranged ferromagnetic spin ordering along the tube.[19] Thus, it is evident that the fluorinated BNNT is a novel metal-free magnetic entity with high conductivity, which makes it a suitable candidate for applications in spin-based electronics (spintronics).[18] The quest for novel metal-free magnetic materials, which exhibit magnetism at a higher temperature, has been intensively pursued since the discovery of magnetic polymerized C_{60}.[20] Despite the desirable properties of fluorinated BNNTs for applications in spintronics, the spin-dependent transport properties in F-BNNT−metal junctions are not yet explored. Understanding the spin-dependent current in such a junction not only depends on the intrinsic electronic and magnetic properties of F-BNNT but also on the electronic structure of the fluorinated BNNT−lead interface.

In this article, using a first-principles approach,[21] we unambiguously confirm the ferromagnetic ordering of spins in the fluorinated BNNT and show that the chemisorption of fluorine on a BNNT quantum dot with a coverage of 4.1% changes the conductance from 6.2 nS to 3.9 μS, which is in very good agreement with the experimental observation. Most importantly, our first-principles quantum transport study predicts that the F-BNNT quantum dot can act as a perfect spin filter with efficiency of 99.8%. Further confinement of electrons in the F-BNNT quantum dot by passivating the two open ends of the channel with hydrogen atoms (weakly coupled junction) leads to additional enhancement of the spin filter efficiency. A minimal change in spin filter efficiency is found with the change in channel length; the change in F coverage from 4.1% to 8.2% is found to alter the spin filter efficiency by a small amount from 99.8% to 99.1%. These

Received: June 8, 2014
Published: July 26, 2014

   dx.doi.org/10.1021/ja505757f | J. Am. Chem. Soc. 2014, 136, 11494−11498

results thus suggest that the observed high spin filter efficiency is a general feature of the F-BNNT.

The rest of the paper is organized as follows. In section 2, we briefly describe our computational methods. Results and discussions are presented in section 3 followed by a brief summary in section 4.

COMPUTATIONAL METHODS

Because BNNTs prefer to adopt a zigzag structure during experimental growth,[22,23] we have considered a representative zigzag BNNT of chirality (6, 0) for our study. A periodic density functional theory (DFT)[21] that employs plane wave basis functions and uses generalized gradient approximation (PW91) for the exchange-correlation is used for the electronic structure calculation of the pristine BNNT. The projected augmented wave (PAW) approach is used to describe the valence−core interaction. We use $1 \times 1 \times 11$ k point grid within the Monkhorst−Pack (MP) scheme to sample the Brillouin zone. Calculations are performed using the Vienna ab initio simulation (VASP) code.[24] The structure is considered optimized when the force on each atom is ≤0.01 eV/Å; the convergence criterion for the energy is 10^{-6} eV. For the fluorinated BNNT, we have used the spin-polarized DFT and have considered a 4.1% coverage of fluorine, i.e., one fluorine atom in the supercell comprising 25 atoms. Our choice of a small F coverage of 4.1% is prompted by a similar low coverage used in the experiment.[15,16]

To study the electron transport property of the fluorinated BNNT, we have constructed a prototypical device by sandwiching a fragment of the F-BNNT (∼1.5 nm length) between two gold electrodes (Figure 1). The experimental measurement of current in the F-BNNT is carried out with gold electrodes.[15] Because electrons are confined in the F-BNNT channel and there is a lattice mismatch between the gold electrode and F-BNNT, we term the channel hereafter as the F-BNNT quantum dot (QD). Because the F-BNNTQD is magnetic in nature, we have adopted a real space approach that allows us to construct the spin-polarized retarded Green's function (G^{σ})[18,25,26] of the open device by dividing it into two parts: (i) the active scattering region consisting of the NTQD together with a finite number of Au atoms from the lead (Figure 1) and (ii) the rest of the electrode on each side which is assumed to retain its bulk (3D) property. Subsequently, a spin-conserved tunneling approach as developed in ref 27 is used to calculate the spin-dependent current in the F-BNNTQD. Spin-up (majority) and spin-down (minority) contributions are the same in the nonmagnetic, pristine BNNTQD−gold junction. A posteriori B3LYP functional, which partly eliminates the self-interaction error by including the exact exchange energy from the Hartree−Fock approach, is used to calculate the electronic structures. The LANL2DZ effective core-potential basis set that includes scalar relativistic effects is used to describe the gold atoms, whereas other relatively light atoms (F, B, N) are represented by the all-electron 6-311 G* basis set.[28] A finite perturbative approach is used to include the bias effect self-consistently.

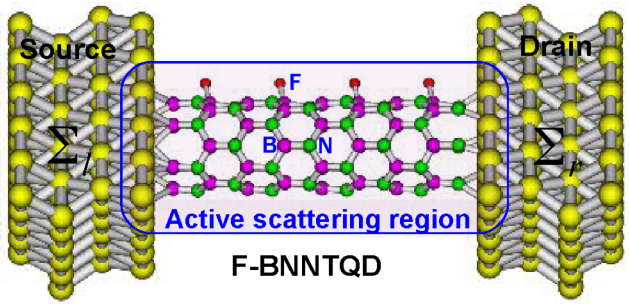

Figure 1. Schematic diagram of a spin-filter with F-BNNTQD as the channel. $\sum_l$ and $\sum_r$ are the self-energy functions that allow the F-BNNTQD to exchange energy and electrons with the semi-infinite gold electrodes of the open device.

RESULTS AND DISCUSSION

First, we focus on the electronic structure calculations of the pristine and fluorinated BNNTs. Our calculation yields a direct band gap of 2.77 eV in the pristine BNNT, which is in line with the previous report.[29] In the case of the F-BNNT, we have considered the most stable exohedral binding of a fluorine atom on top of a boron atom (see Supporting Information), which has been reported to be the most favorable configuration.[16,17,19,30] The binding energy E_b, defined as $E_b = [E_{BNNT} + E_F - E_{F\text{-}BNNT}]$ for this most stable configuration, is found to be 3.02 eV; E_{BNNT}, E_F, and $E_{F\text{-}BNNT}$ are the energies of the pristine BNNT, F atom, and fluorinated BNNT, respectively. Structure optimization of the F-BNNT shows a F atom bringing the B atom to which it is bonded out of the surface (see Supporting Information), resulting in an increased B−N bond length near the adsorption site. This local deformation changes the sp^2 hybridization of a B atom in the pristine BNNT to the sp^3 hybridization in the F-BNNT. A similar fluorine-induced hybridization change for the C atom has been observed in the F-CNT.[31] For a 4.1% fluorine coverage, the fluorinated BNNT is found to be magnetic with a total magnetic moment of 1.0 μ_B for one F atom in the unit cell; the unpaired electrons at the N atoms in the vicinity of the adsorbed F atom created by the loss of some electrons from it to the highly electronegative F atom contribute to the magnetism. We double the size of the supercell with the same coverage of F and perform spin-polarized electronic structure calculations to check for the stability of the ferromagnetic ordering in the fluorinated BNNT. The ferromagnetic (FM) configuration is found to be more stable (by 15 meV) than the antiferromagnetic configuration (AFM), which is in excellent agreement with the previously reported value.[19]

To check for the thermodynamic stability of the FM state, we have calculated the energy barrier by finding the energy difference between the metastable paramagnetic state (expected transition point between the FM and AFM states) and the stable FM state. The energy barrier is found to be 1.6 eV, which is much higher than the room temperature (26 meV). To examine if this FM behavior of F-BNNT persists for a higher F coverage, we increase the F coverage to 16.4% by including four F atoms in the unit cell; the supercell used for our calculations consists of two unit cells with eight F atoms. The FM configuration is found to be much more stable (by 0.11 eV) than the AFM configuration as noted for the 4.1% F coverage. However, the barrier height between the FM and AFM states decreases to 0.61 eV. Though the barrier height for the 16.4% F coverage is smaller than that observed for the 4.1% F coverage, it is still much higher (∼23 times) than the room temperature. This result thus ensures that the stable FM state in F-BNNT cannot be inadvertently switched to the AFM state at a higher temperature , *an important characteristic of a metal-free magnetic entity*. It is important to note that the magnetic property of the fluorinated BNNT is different from that of the fluorinated BN sheet. In the F-BN sheet, both the FM and AFM states are found to be nearly degenerate.[32] Curvature-induced stress in the F-BNNT is responsible for the ferromagnetic ordering.[32]

Next, we turn to current (I)−voltage (V) calculations in the BNNT and F-BNNT quantum dots, which is the main focus of the present investigation. Figure 2 summarizes the calculated $I-V$ characteristics. Because F-BNNT is magnetic, the total

dx.doi.org/10.1021/ja505757f | J. Am. Chem. Soc. 2014, 136, 11494−11498

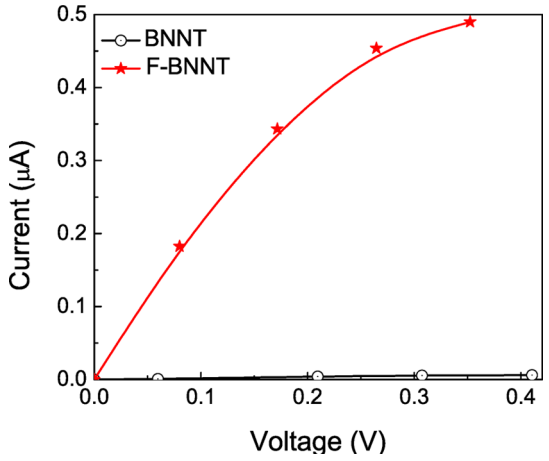

Figure 2. $I-V$ characteristics of the pristine BNNTQD and F-BNNTQD coupled to the metallic gold electrodes; channel length is ∼1.5 nm.

current for this system is obtained by adding the spin-up (majority) current ($I_\uparrow$) and spin-down (minority) current ($I_\downarrow$). The current in the F-BNNTQD is found to be significantly higher than that of the pristine BNNTQD at the same bias. For example, at V = 0.06 V, the current for the F-BNNTQD is found to be 0.13 μA, which is 153 times higher than that of the pristine BNNTQD. This result is in good agreement with the experimental report,[15] which shows a three order lower resistance in the fluorinated BNNT as compared to that in the pristine BNNT.

To gain a deeper understanding of the observed higher current in F-BNNTQD, we examine up (↑) and down (↓) spin states contributions to the total current (Figure 3). $I_\downarrow$ is found

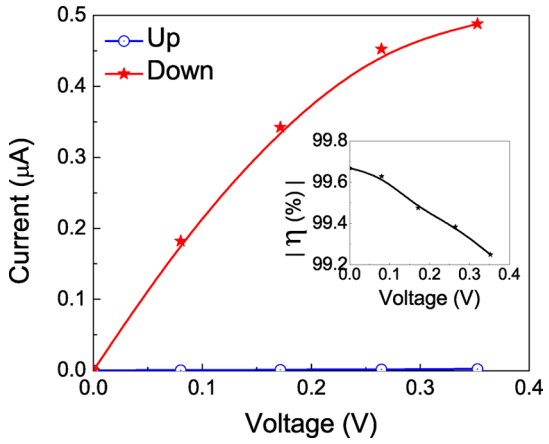

Figure 3. Bias-dependent spin-up and spin-down contributions to current in the fluorinated BNNTQD. The inset shows the variation of the magnitude of spin injection coefficient (η) with bias; channel length is ∼1.5 nm. Up and Down refer to majority and minority spin states, respectively.

to be appreciably larger than $I_\uparrow$. To quantify the difference between $I_\uparrow$ and $I_\downarrow$ in the F-BNNTQD, we have calculated the spin injection factor (η) as $(I_\uparrow - I_\downarrow)/(I_\uparrow + I_\downarrow)$. The inset of Figure 3 shows the variation of magnitude of η as a function of applied bias. Within the bias range considered here, a small variation (∼0.4%) of η with bias is noted. The maximum magnitude of the η value is found to be 99.76%. For zero bias, the η value is obtained as $(T_\uparrow(E_f) - T_\downarrow(E_f))/(T_\uparrow(E_f) + T_\downarrow(E_f))$ × 100%, where $T_\uparrow$ and $T_\downarrow$ are the transmission coefficients for spin-up and spin-down channels, respectively (Figure 4); the

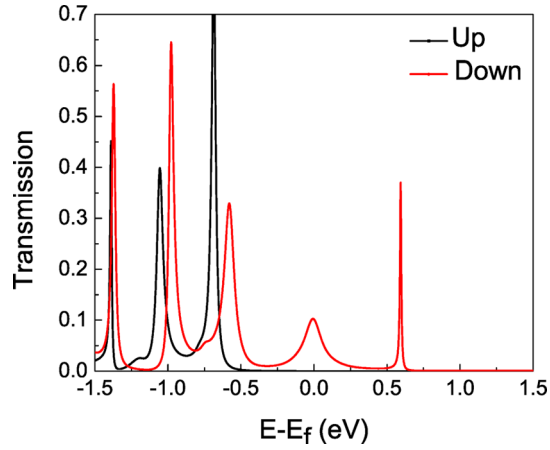

Figure 4. Spin-dependent transmission in the F-BNNTQD−gold junction; the F coverage is 4.1% and the channel length is ∼1.5 nm. Up and Down refer to majority and minority spin states, respectively.

zero bias η value is referred to as the spin filter efficiency. To see how the length of the F-BNNT channel affects the spin filter efficiency, we have recalculated the spin-dependent transmission for a longer channel length of about 2 nm (Figure 5). The same interface geometry as that of the shorter channel length is considered.

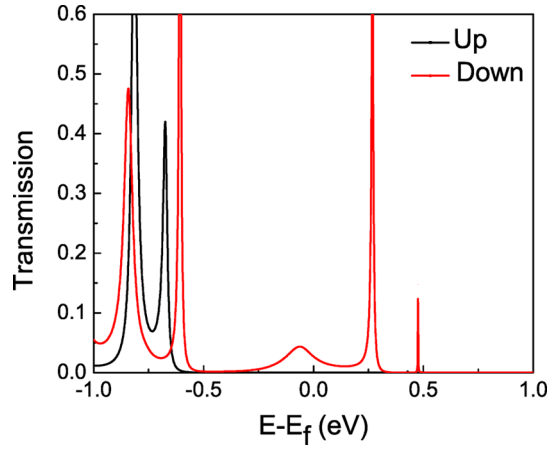

Figure 5. Spin-dependent transmission in the F-BNNTQD−gold junction for the channel length of ∼2 nm and F coverage of 4.1%. Up and Down refer to majority and minority spin states, respectively.

Though the height of the transmission values for both the up and down spin states decrease at the Fermi energy for the longer channel length as expected in the tunneling regime, the spin filter efficiency is found to be 99.9%, which is much closer to that observed for the shorter channel length. Thus, this result confirms that the observed high spin filter efficiency is a general feature of the F-BNNT channel (within the limit of spin coherence length). The observed high value of η together with a very small variation with bias (see inset of Figure 3) makes the F-BNNTQD a potential spin filter candidate. We have also calculated the spin-dependent transmission for a 8.2% coverage of F on the BNNT to examine the dependence of F adsorbates on the spin filter efficiency. The results are shown in Figure 6.

dx.doi.org/10.1021/ja505757f | J. Am. Chem. Soc. 2014, 136, 11494−11498

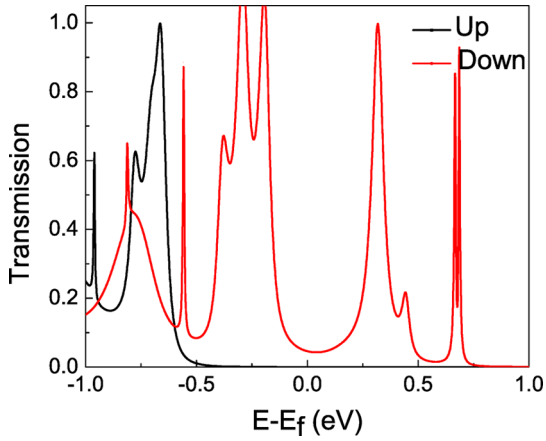

Figure 6. Spin-dependent transmission in the F-BNNTQD−Au junction; F coverage is 8.2% and channel length is ∼1.5 nm. Up and Down refer to majority and minority spin states, respectively.

Despite some noticeable changes in transmission features around the Fermi energy between the QDs with 4.1% and 8.2% F coverage, the transmission from the minority spin states for the 8.2% F coverage is found to be significantly higher than that of the majority spin states at the Fermi energy as noted for the 4.1% F coverage (Figure 4). The spin filter efficiency is found to be 99.1%, which is slightly smaller than that observed for a 4.1% F coverage. For a longer channel length of ∼2 nm (with 8.2% F coverage), the spin filter efficiency is found to be ∼1; the transmission from the up state at the Fermi energy completely vanishes. Thus, our result of high spin filter efficiency is valid for a reasonably small F coverage irrespective of channel length.

To simulate a possible defect in the experimental situation, we have removed one fluorine atom from the F-BNNT with a 8.2% F coverage (12.5% defect) and have recalculated the spin-dependent transmission (Figure 7). The FM ordering of spins is found to be the most stable configuration for this defect state with a barrier height of 0.11 eV between the FM and AFM states. From Figure 7, though a significant change in the transmission feature with defects is observed as expected in a chemisorbed system, the transmission from the spin-down states is again found to be significantly higher than that of the spin-up states at the Fermi energy similar to that in a defect-free F-BNNTQD (Figure 6). The spin filter efficiency is found to be 98.7%, which is slightly smaller than that observed for the defect-free F-BNNTQD. The spin injection efficiency has been reported to depend sensitively on the interface; a strongly coupled junction structure has been found to exhibit a lower η value compared to that in a weakly coupled junction.[33] To check if the F-BNNTQD exhibits such behavior, we have recalculated the spin-dependent transmission in a weakly coupled junction structure. To mimic the weak coupling effect at the interface, we have terminated the F-BNNTQD at both interfaces by hydrogen atoms. Our results for the hydrogen-terminated F-BNNTQD indeed show a higher spin injection factor of 99.96% at equilibrium, which is in good agreement with the earlier observation.[33]

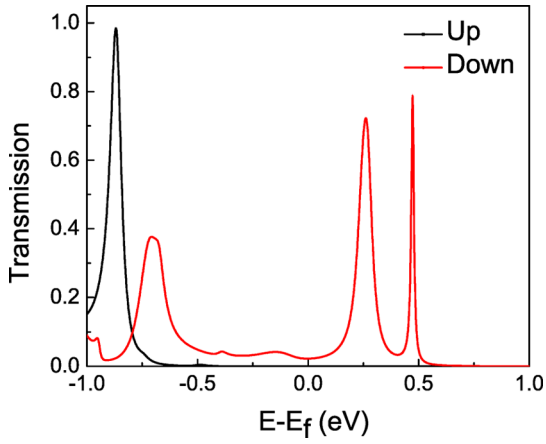

Figure 7. Spin-dependent transmission in the F-BNNTQD−Au junction with a 12.5% defect; F coverage is 8.2% and channel length is ∼1.5 nm. Up and Down refer to majority and minority spin states, respectively.

Our analysis of transmission coefficients show that in the case of nonmagnetic pristine BNNTQD, no transmission peaks are found around the Fermi energy for the bias range considered here; the transmission values in the vicinity of the Fermi energy is found to be very small (8×10^{-5}). This explains the much smaller observed current in the pristine BNNTQD. In contrast, for the magnetic F-BNNTQD, distinct spin-dependent transmission peaks are noticeable (Figure 4). For the spin-up state, the transmission peak, which is closest to the Fermi energy, is observed at −0.8 eV. This transmission peak does not contribute to $I_{\uparrow}$ for the small bias window [0, 0.4]. However, for the spin-down state, a broadened transmission peak appears at the Fermi energy. This leads to an appreciably higher $I_{\downarrow}$ in the case of F-BNNTQD. Within the linear response regime, the conductance value can be inferred from the transmission data at the Fermi energy as $G = ((e)^2/h) \times T(E_F; V = 0)$. In the case of F-BNNTQD, we find the value of G to be 3.9 μS, which is about 3 orders higher than that of the pristine BNNTQD. This change in conductance is not only in good agreement with the experimental report but also reaffirms our previous observation of more than 2 orders of magnitude difference in current between the pristine and fluorinated BNNTQDs. A similar significant change in the conductance value with chemical functionalization of CNT by different molecular adsorbates has been reported.[34,35]

To understand the transmission features of the fluorinated BNNTQD at the Fermi-energy, we have analyzed the frontier orbitals of the extended system, which provide the spatial pathway for the spin-polarized charge carriers. For the spin-down channel, the highest occupied system orbital (HOSO) having contribution from *both interfaces* (s-orbitals from Au−lead and p-orbitals from B and N) contribute to the transmission at the Fermi energy. In contrast, only *one interface* contributes to $T(E_f)$ for the spin-up channel. A close examination of HOSO for spin-down state shows that in addition to the interface states, the p-orbitals of the nitrogen in the close vicinity of adsorbed fluorine atoms in the F-BNNTQD provides the route for spin-down electrons. For the spin-up channel, no such route exists. The broadened feature of the transmission peak at the Fermi energy for the spin-down channel can be understood from the strong coupling between s-states of Au and p-states of N and B at the interfaces.

On the basis of the above discussions, the spin filtering mechanism for the F-BNNTQD can be visualized as shown in Figure 8. Because the F-BNNTQD is magnetic, the energy levels are quantized and spin polarized. When we form the junction between F-BNNTQD and the nonmagnetic gold

dx.doi.org/10.1021/ja505757f | J. Am. Chem. Soc. 2014, 136, 11494−11498

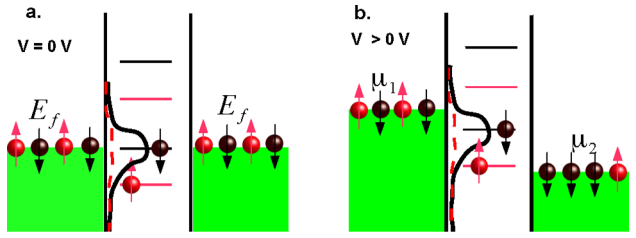

Figure 8. Mechanism behind spin filtering in the F-BNNTQD. Horizontal lines represent the position of the discrete spin-polarized energy levels of the magnetic F-BNNTQD. The solid, smooth curved line represents the density of states (DOS) around the Fermi energy for the spin-down states due to coupling with the gold electrodes; the dotted line represents the DOS for the spin-up states. (a) $V = 0$ V (equilibrium situation), and (b) $V > 0$ V.

electrodes, the energy levels of the F-BNNTQD for both the up and down spin states redistribute and broaden with a different strength (Figure 8) depending upon the applied bias and the coupling with the interface. The highest occupied molecular orbital (HOMO) of spin-down channels not only gets closer to the Fermi energy but also gets broadened significantly in comparison to the HOMO of the spin-up channels during the junction formation; this enhances the escape rate of the spin-down electrons from source to drain, resulting in a significantly higher $I_{\downarrow}$ compared to $I_{\uparrow}$ in the F-BNNTQD.

SUMMARY

Using a first-principles approach, we have shown the conductance of the fluorinated BNNTQD to be more than 2 orders higher than that of the pristine BNNTQD, which is in very good agreement with the experimental report. Furthermore, we predict that the fluorinated BNNT, which exhibits long-range ferromagnetic spin ordering at a temperature above the room temperature, can be used as an ideal spin filter with efficiency higher than 99%. We expect that these novel findings will generate fresh experimental initiative toward the realization of a next generation spin filter device based upon fluorinated BNNTs.

ASSOCIATED CONTENT

Supporting Information

Structures and coordinates of the atoms in the unit cells. This material is available free of charge via the Internet at http://pubs.acs.org.

AUTHOR INFORMATION

Corresponding Author

patir@mtu.edu

Notes

The authors declare no competing financial interest.

ACKNOWLEDGMENTS

This work is supported by the NSF through grant no. 1249504. The results reported here were obtained using RAMA and Superior, the high performance computing clusters at Michigan Technological University.

REFERENCES

(1) Iijima, S. *Nature* **1991**, *56*, 354.
(2) Rubio, A.; Corkill, J. L.; Cohen, M. L. *Phys. Rev. B* **1994**, *49*, 5081.
(3) Blase, X.; Rubio, A.; Louie, S. G.; Cohen, M. L. *Eur. Phys. Lett.* **1994**, *28*, 335.
(4) Chopra, N. G.; Luyken, R. J.; Cherrey, K.; Crespi, V. H.; Cohen, M. L.; Louie, S. G.; Zettl, A. *Science* **1995**, *269*, 966.
(5) Golberg, D.; Bando, Y.; Huang, Y.; Terao, T.; Mitome, M.; Tang, C.; Zhi, C. *ACS Nano* **2010**, *4*, 2979.
(6) Ishigami, M.; Aloni, S.; Zettl, A. *AIP Conf. Proc.* **2003**, *696*, 9499.
(7) Zhi, C. Y.; Bando, Y.; Tang, C. C.; Huang, Q.; Golberg, D. *J. Mater. Chem.* **2008**, *18*, 3900.
(8) Tang, C.; Bando, Y.; Sato, T.; Kurashima, K. *Chem. Commun.* **2002**, *12*, 1290.
(9) Chen, J.; Liu, H.; Weimer, W. A.; Halls, M. D.; Waldeck, D. H.; Walker, G. C. *J. Am. Chem. Soc.* **2002**, *124*, 9034.
(10) Fukushima, T.; Kosaka, A.; Ishimura, Y.; Yamamoto, T.; Takigawa, T.; Ishii, N.; Aida, T. *Science* **2003**, *300*, 2072.
(11) Han, W.-Q.; Zettl, A. *J. Am. Chem. Soc.* **2003**, *125*, 2062.
(12) Mukhopadhyay, S.; Gowtham, S.; Scheicher, R. H.; Pandey, R.; Karna, S. P. *Nanotechnology* **2010**, *21*, 165703.
(13) Mukhopadhyay, S.; Scheicher, R. H.; Pandey, R.; Karna, S. P. *J. Phys. Chem. Lett.* **2011**, *2*, 2442.
(14) Lau, Y-T. R.; Yamaguchi, M.; Li, X.; Bando, Y.; Golberg, D.; Winnik, F. M. *J. Phys. Chem. C* **2013**, *117*, 19568.
(15) Tang, C.; Bando, Y.; Huang, Y.; Yue, S.; Gu, C.; Xu, F.; Golberg, D. *J. Am. Chem. Soc.* **2005**, *127*, 6552.
(16) Zhao, J.; Li, W.; Tang, C.; Li, L.; Lin, J.; Gu, C. *Appl. Phys. Lett.* **2013**, *102*, 153107.
(17) Li, F.; Zhu, Z.; Yao, X.; Lu, G.; Zhao, M.; Xia, Y.; Chen, Y. *Appl. Phys. Lett.* **2008**, *92*, 102515.
(18) Dhungana, K. B.; Pati, R. *Phys. Chem. Chem. Phys.* **2014**, *16*, 7996.
(19) Zhang, Z.; Guo, W. *J. Am. Chem. Soc.* **2009**, *131*, 6874.
(20) Makarova, T. L.; et al. *Nature* **2001**, *413*, 716.
(21) Parr, R. G.; Yang, W. *Density-Functional Theory of Atoms and Molecules*; Oxford Science: Oxford, 1994.
(22) Terauchi, M.; Tanaka, M.; Suzuki, K.; Ogino, A.; Kimurab, K. *Chem. Phys. Lett.* **2000**, *324*, 359.
(23) Golberg, D.; Y. Bando, Y.; Bourgeois, L.; Kurashima, K.; Sato, T. *Appl. Phys. Lett.* **2000**, *77*, 1979.
(24) VIENNA ab initio Simulation Package, Technishche Universität Wien, 1999. Kresse, G.; J. Furthmüller *Phys. Rev. B* **1996**, *54*, 11169.
(25) Waldron, D.; Haney, P.; Larade, B.; MacDonald, A.; Guo, H. *Phys. Rev. Lett.* **2006**, *96*, 166804.
(26) Herrmann, C.; Solomon, G. C.; Ratner, M. A. *J. Am. Chem. Soc.* **2010**, *132*, 3682.
(27) Mandal, S.; Pati, R. *ACS Nano* **2012**, *4*, 3580.
(28) *GAUSSIAN 09, revision A.1*, Gaussian, Inc., Wallingford, CT, 2009.
(29) Kinoshita, Y.; Ohno, N. *Phys. Rev. B* **2010**, *82*, 085433.
(30) Zhou, Z.; Zhao, J.; Chen, Z.; Schleyer, P. R. *J. Phys. Chem. B* **2006**, *110*, 25678.
(31) Park, K. A.; Choi, Y. S.; Lee, Y. H.; Kim, C. *Phys. Rev. B* **2003**, *68*, 045429.
(32) Zhou, J.; Wang, Q.; Sun, Q.; Jena, P. *Phys. Rev. B* **2010**, *81*, 085442.
(33) Kondo, H.; Ohno, T. *Appl. Phys. Lett.* **2013**, *103*, 233115.
(34) García-Lastra, J. M.; Thygesen, K. S.; Strange, M.; Rubio, A. *Phys. Rev. Lett.* **2008**, *101*, 236806.
(35) García-Lastra, J. M.; Mowbray, D. J.; Thygesen, K. S.; Rubio, A.; Jacobsen, K. W. *Phys. Rev. B* **2010**, *81*, 245429.